CellPress
Structure
Article

Structural Insights into FGFR Kinase Isoform Selectivity: Diverse Binding Modes of AZD4547 and Ponatinib in Complex with FGFR1 and FGFR4

Julie A. Tucker,[1,2,3] Tobias Klein,[1,2,4] Jason Breed,[1] Alexander L. Breeze,[1,5] Ross Overman,[1] Chris Phillips,[1] and Richard A. Norman[1,*]
[1]Discovery Sciences, AstraZeneca, Mereside, Alderley Park, Macclesfield, Cheshire SK10 4TG, UK
[2]Co-first author
[3]Present address: Northern Institute for Cancer Research, Paul O'Gorman Building, Medical School, Newcastle University, Framlington Place, Newcastle upon Tyne NE2 4HH, UK
[4]Present address: Bayer Healthcare, Emil-Barell Strasse 7, 79639 Grenzach-Whylen, Germany
[5]Present address: The Faculty of Biological Sciences, University of Leeds, Leeds LS2 9JT, UK
*Correspondence: richard.norman@astrazeneca.com
http://dx.doi.org/10.1016/j.str.2014.09.019

SUMMARY

The fibroblast growth factor receptor (FGFR) family of receptor tyrosine kinases has been implicated in a wide variety of cancers. Despite a high level of sequence homology in the ATP-binding site, the majority of reported inhibitors are selective for the FGFR1-3 isoforms and display much reduced potency toward FGFR4, an exception being the Bcr-Abl inhibitor ponatinib. Here we present the crystal structure of the FGFR4 kinase domain and show that both FGFR1 and FGFR4 kinase domains in complex with ponatinib adopt a DFG-out activation loop conformation. Comparison with the structure of FGFR1 in complex with the candidate drug AZD4547, combined with kinetic characterization of the binding of ponatinib and AZD4547 to FGFR1 and FGFR4, sheds light on the observed differences in selectivity profiles and provides a rationale for developing FGFR4-selective inhibitors.

INTRODUCTION

The fibroblast growth factor (FGF)-FGF receptor (FGFR) signaling system plays important roles in development and tissue repair through the initiation of multiple signaling cascades controlling proliferation, differentiation, migration, and survival (Brooks et al., 2012; Turner and Grose, 2010). Dysregulation of this signaling axis has been shown to play a critical role in tumor development and progression. Activating mutations in members of the FGFR tyrosine kinase family (FGFR1, FGFR2, FGFR3, and FGFR4) are emerging as significant markers of a number of human cancers and other diseases (Greulich and Pollock, 2011).

FGFR4 is activated by the binding of the extracellular growth factors FGF1 and FGF19 to the extracellular domains of the transmembrane receptor, an event that results in receptor dimerization. Upon receptor dimerization, the intracellular tyrosine kinase domains undergo autophosphorylation, resulting in further activation of basal tyrosine kinase activity, leading to phosphorylation and activation of its intracellular substrates (FGFR substrate 2α and phospholipase Cγ1) and initiation of downstream signaling pathways (RAS-MAPK, PI3K-AKT, and PKC) (Goetz and Mohammadi, 2013). In addition, FGFR4 can activate other signaling molecules, including signal transduction and activation of transcription (Hart et al., 2000). The FGFR4-FGF19 complex is further stabilized by binding of the tissue-specific coreceptor β-Klotho (Kurosu et al., 2007; Lin et al., 2007; Wu et al., 2010). Overexpression of FGFR4, FGF1, and FGF19 and activating mutations in FGFR4 (e.g., Gly388Arg) have been associated with poor prognosis in a wide variety of tumor types, such as breast, colon, and lung adenocarcinomas (Bange et al., 2002; Spinola et al., 2005a, 2005b; Thussbas et al., 2006); hepatocellular carcinoma (Ho et al., 2009; reviewed in Mellor, 2014); serous ovarian cancer (Birrer et al., 2007; Zaid et al., 2013); rhabdomyosarcoma (RMS) (Taylor et al., 2009), and pancreatic (Chen et al., 2010a), colorectal, and gastric cancers (Jang et al., 2001; Ye et al., 2011). A number of germline and somatic mutations in *FGFR4* identified in tumor samples have been shown to both increase FGFR4 signaling and drive cell proliferation in model systems, further supporting the role of FGFR4 in oncogenic progression (Roidl et al., 2010; Ruhe et al., 2007; Taylor et al., 2009).

The potential of targeting FGFR4 as a therapeutic intervention is supported by promising data for a number of biopharmaceutical agents targeting the FGF19-FGFR4 interaction. An anti-FGFR4 monoclonal antibody (LD1) that inhibits binding of FGF ligands (FGF19 and FGF1) to FGFR4 has been shown to inhibit proliferation in vitro and in preclinical models of liver cancer (French et al., 2012). Inhibition of FGF19-FGFR4 signaling in colon cancer using an alternative FGF19-blocking antibody (IA6) has been shown to inhibit the growth of HCT116 and Colo201 xenograft tumors (Desnoyers et al., 2008). In a repeat-dose safety study in cynomolgus monkeys, however, anti-FGF19 treatment exhibited dose-related liver toxicity (Pai et al., 2012). FGFR4 function is not essential during embryogenesis or adult life in mice (Weinstein et al., 1998), suggestive of a favorable therapeutic margin. FGFR4 function is, however, required for the correct regulation of bile acid synthesis via Cyp7A1, and inhibition of FGFR4 has been shown to result in bile acid malabsorption (reviewed in Mellor, 2014). A recent study using both

FGFR4-targeted small interfering RNA and the small-molecule pan-FGFR kinase inhibitor BGJ398 indicated that FGFR4 is a targetable regulator of chemoresistance in advanced colorectal cancer and that inhibition of FGFR4 in combination with the antimetabolite 5-fluorouracil and the DNA-damaging agent oxaliplatin may present a potential therapeutic strategy for this indication (Turkington et al., 2014). Further dissection of the role of FGFR4 kinase activity in normal and aberrant physiological processes and its relevance as a therapeutic target is hampered by the lack of FGFR4-selective small-molecule kinase inhibitors. Development of such inhibitors would, in turn, be assisted by the availability of structural information on the kinase domain of FGFR4. Structures of the kinase domains of FGFR1 (Mohammadi et al., 1996), FGFR2 (Chen et al., 2007), and FGFR3 (Huang et al., 2013) have been described, but until now, that of FGFR4 has not been reported.

The majority of reported small-molecule FGFR inhibitors for which in vitro pan-isoform selectivity data are available display much reduced potency toward FGFR4 compared to FGFR1-3 (Ho et al., 2014). The pyrazole derivative AZD4547, a selective inhibitor of FGFR tyrosine kinases currently in phase II clinical trials (ClinicalTrials.gov identifier NCT01457846) for the treatment of FGFR-dependent tumors, shows single-digit nanomolar inhibition of FGFR1-3 in an enzyme assay. Its half maximal inhibitory concentration (IC_{50}) for isolated FGFR4, however, is markedly reduced (1,000-fold) (Gavine et al., 2012). In contrast, the multitargeted tyrosine kinase inhibitor (TKI) ponatinib (AP24534), which has been shown to bind the "DFG-out" conformation of Bcr-Abl (Zhou et al., 2011), shows potent pan-FGFR activity (Gozgit et al., 2012). In the DFG-out conformation, the Phe side chain (the F of the DFG motif) is flipped out of its hydrophobic pocket, and targeting of this pocket adjacent to the ATP-binding site is characteristic for type II inhibitors. In contrast, type I inhibitors bind competitively with ATP and do not require a flip of the DFG motif for binding (Norman et al., 2012b; Liu and Gray, 2006). To date, all reported FGFR-inhibitor complex structures show binding to a "DFG-in" conformation of the kinase domain in which the Phe side chain is in a conformation compatible with ATP binding.

The conformation of the DFG motif is one defining feature of the active versus inactive state. Additional features of active kinase structures include the so-called hydrophobic spine, comprising four highly conserved hydrophobic residues (Leu536, Met524, His610, and Phe631 in FGFR4) (Kornev et al., 2006). In the active state, interactions between these residues link the gatekeeper residue (Liu et al., 1998) (Val550 in FGFR4) to the phosphorylated tyrosine (Tyr643 in FGFR4) of the activation loop. The gatekeeper residue lies at the beginning of the hinge region linking the N- and C-terminal lobes of the kinase domain. Activating mutations in the gatekeeper residue of SRC, EGFR, and Abl kinases have been proposed to stabilize the hydrophobic spine through improved packing (Azam et al., 2008). In addition, FGFR kinase activity is controlled by a network of hydrogen bonds between conserved residues (Glu551, Asn535, and Lys627 in FGFR4) in the vicinity of the hinge region termed the "molecular brake" (Chen et al., 2007). This network restricts the interlobe closure required for the productive alignment of catalytic residues. Disease-associated mutations of key residues in this network have been described in all FGFR isoforms, including FGFR4 (reviewed in Greulich and Pollock, 2011). These mutations lead to inappropriate activation of FGFR kinase activity mediated through disengagement of the "brake" (Chen et al., 2007). Activating mutations in the gatekeeper and molecular brake residues have also been associated with chemoresistance in a number of kinases, including FGFRs (Byron et al., 2013; O'Hare et al., 2007).

In an attempt to understand isoform- and inhibitor-dependent differences at a molecular level, we have solved the structures of FGFR4 in complex with ponatinib and of FGFR1 in complex with both AZD4547 and ponatinib. Here we reveal that FGFR, in common with a diverse subset of kinases, including p38 (Protein Data Bank [PDB] accession number 1KV2), cAbl (PDB accession number 1OPJ), Aurora kinase (PDB accession number 2C6E), CDK8 ("DMG-out"; PDB accession number 3RGF), and MNK ("DFD-out"; PDB accession number 2AC3), can adopt a DFG-out activation loop conformation. Comparisons of the AZD4547 and ponatinib binding modes and accompanying binding kinetics determined using surface plasmon resonance (SPR) provide insight into the molecular determinants governing inhibitor-dependent potency differences toward FGFR1 and FGFR4 kinases. We discuss the implications of our findings for the design of FGFR4 isoform-selective TKIs.

RESULTS

The Structure of FGFR4 in Complex with Ponatinib Reveals a DFG-Out Binding Mode

In order to understand the molecular basis by which FGFR4-selective inhibitors may be developed, we began by determining the crystal structure of the kinase domain of FGFR4. We designed a series of constructs encompassing the kinase domain of FGFR4, including both wild-type sequences and also incorporating a Cys477Ala mutation in the glycine-rich loop by analogy with the construct used to obtain crystals of FGFR1 (Mohammadi et al., 1996). Purified FGFR4 showed heterogeneous phosphorylation at up to four sites, and no crystals were obtained from this sample. In order to improve sample homogeneity, we coexpressed FGFR4 with PTP1B to generate nonphosphorylated FGFR4. In the absence of ligand, FGFR4 failed to crystallize despite extensive screening, we therefore used differential scanning fluorimetry to assess the effect of a variety of potential FGFR4 ligands on the protein melting temperature (Tm) in order to identify conditions more likely to result in crystal formation (Niesen et al., 2007). Both Cys477Ala and wild-type, phosphorylated, and nonphosphorylated FGFR4 showed significant stabilization (monitored as an increase in Tm) in the presence of a variety of FGFR inhibitor chemotypes (Table S1 available online; data not shown). The largest stabilization (+11.1 ± 0.4 K) was observed in the presence of the multitargeted TKI ponatinib, and diffraction quality crystals were obtained for the complex of nonphosphorylated FGFR4 (Ala447-Glu753 [Cys477Ala]) with ponatinib. Compounds showing lower Tm shifts failed to yield diffraction quality crystals. Data were collected from several crystals of the FGFR4-ponatinib complex harvested from the initial screening condition and showed variable diffraction quality. In order to maximize the data resolution and completeness, data from three crystals were combined to give an overall resolution limit of 1.85 Å (Table 1; Experimental

Table 1. Crystallographic Data Collection and Refinement Statistics

Protein	FGFR1 (458–765) [C488A C584S]	FGFR1 (458–765) [C488A C584S]	FGFR1 (458–765) [C488A C584S]	FGFR4 (447–753) [C477A]
Ligand	ponatinib	ponatinib	AZD4547	ponatinib
PDB accession number	4V01	4V04	4V05	4UXQ
Ligand introduction method	soak	cocrystallization	soak	cocrystallization
X-ray source	Rigaku FRE rotating anode	Rigaku FRE rotating anode	Rigaku FRE rotating anode	Diamond i04-1 and ESRF ID29
Wavelength (Å)	1.54	1.54	1.54	0.89 and 0.92
Space group	C2	C2	C2	$P2_1$
Cell constants a; b; c (Å)	207.2; 58.1; 65.2 β = 107.4°	206.8; 57.5; 65.6 β = 107.5°	208.8; 57.5; 65.6 β = 107.6°	41.8; 58.4; 60.6 β = 96.5°
Resolution range (Å)[a]	98.89–2.33 (2.45–2.33)	98.62–2.12 (2.29–2.12)	99.48–2.57 (2.71–2.57)	60.18–1.85 (1.95-1.85)[f]
Completeness overall (%)[a]	94.2 (83.7)	97.7 (90.1)	96.8 (97.1)	56.9 (8)[e]
Reflections, unique	30,021	41,149	22,994	14,141
Multiplicity[a]	2.3 (2.3)	3.5 (2.7)	3.7 (3.8)	4.6 (2.6)
Mean (I)/SD (I)[a]	18.2 (5)	21.5 (3.1)	15.2 (2.7)	7.3 (2.6)
R_{merge} overall[a,b]	0.033 (0.20)	0.042 (0.379)	0.057 (0.458)	0.18 (0.287)
R_{value} overall (%)[c]	19.6	18.81	19.55	20.14
R_{value} free (%)[c]	24.4	22.80	25.56	26.81
Nonhydrogen protein atoms	4308	4594	4439	2241
Nonhydrogen ligand atoms	78	78	68	39
Solvent molecules	277	420	143	229
Rmsd values from ideal values				
Bond length (Å)	0.007	0.010	0.010	0.010
Bond angle (°)	1.19	1.05	1.12	1.12
Average *B* values (Å^2)				
Protein main-chain atoms	28.7	47.7	54.1	21.1
Protein all atoms	29.4	49.9	55.9	23.7
Ligand	30.2	38.4	52.0	17.3
Solvent	42.8	57.5	50.5	27.2
Φ, Ψ angle distribution for residues[d]				
In most favored regions (%)	93.2	92.6	93.5	91.3
In additional allowed regions (%)	6.4	6.8	6.0	8.3
In generously regions (%)	0.4	0.6	0.4	0.4
In disallowed regions (%)	0.0	0.0	0.0	0.0

[a]Values in parentheses refer to the outer resolution shell.
[b]$R_{merge} = S_{hkl}[(\Sigma_i|I_i - \langle I\rangle|)/\Sigma_i I_i]$.
[c]$R_{value} = S_{hkl}||F_{obs}| - |F_{calc}||/S_{hkl}|F_{obs}|$. R_{value} free is the cross-validation *R* factor computed for the test set of 5% of unique reflections.
[d]Ramachandran statistics as defined by PROCHECK (Laskowski et al., 1993).
[e]Overall completeness to 2.4 Å is 90% and to 2.2 Å is 84%.
[f]Data collection and processing statistics are given for the merged data set, combining data from three individual crystals.

Procedures). The structure was solved by molecular replacement, initially using a low-resolution structure of FGFR4 and subsequently using a high-resolution structure of FGFR1 (Supplemental Experimental Procedures).

The refined model consists of residues Leu452 to Val750, the inhibitor and 229 water molecules (see Table 1 for detailed statistics of the refinement and final model quality). FGFR4 exhibits the canonical two-domain architecture of protein kinases; a smaller N-terminal domain comprising a five-stranded β sheet and the αC-helix and a larger, predominantly α helical C-terminal domain (Figure 1A).

The structure of the FGFR4 kinase domain is highly homologous to that of other FGFR family members, with root-mean-square deviation (rmsd) values of 1.06, 1.31, and 1.41 Å over the αC's of the 266, 268, and 263 corresponding residues in FGFR1 (PDB accession number 1FGK), FGFR2 (PDB accession number 2PSQ), and FGFR3 (PDB accession number 4K33), which show sequence identities of 74%, 75%, and 77%, respectively. The entire activation loop, comprising residues Ile628 to Pro652, is ordered including the tyrosine residues Tyr642 and Tyr643, which become phosphorylated upon activation. It should be noted that the ordered activation loop in FGFR4 packs

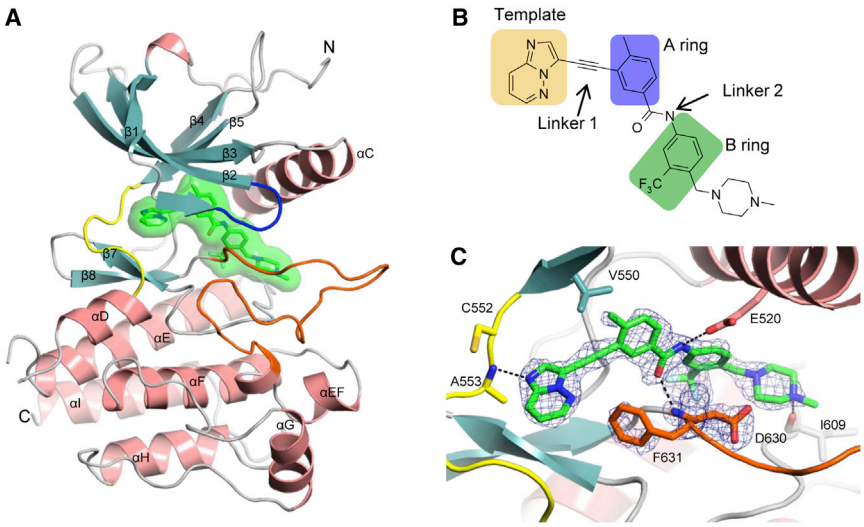

Figure 1. Crystal Structure of the Catalytic Domain of FGFR4 Kinase in Complex with Ponatinib

(A) Ribbon representation of the X-ray crystal structure of FGFR4 in complex with ponatinib (carbon atoms in green, van der Waals surface representation also shown). The termini are denoted by N and C; β strands and α helices are labeled and numbered. The hinge region (yellow), P loop (blue), and activation loop (orange) are highlighted.

(B) 2D chemical representation of ponatinib, which is composed of several motifs designated as the (imidazopyridazine) template, the (methylphenyl) A ring and (trifluoromethylphenyl) B ring, as well as the two linkers (Zhou et al., 2011).

(C) Active site of FGFR4 kinase in complex with ponatinib (carbon atoms in green) as determined at 1.85 Å resolution. $F_o - F_c$ OMIT electron density map for ponatinib and the DFG motif is represented as a blue mesh contoured at 3.0σ. Polar interactions are indicated as dotted lines. Selected residues are represented as sticks and labeled.

against a symmetry-related molecule making extensive contacts. A loop-turn-helix motif formed by residues 704 to 728 (from the linker connecting helices αG and αH and helix αH) of the symmetry-related molecule packs against the C-terminal lobe, masking from solvent a hydrophobic surface patch formed by residues Leu661, Phe662, and Phe669. The side chain of Asp709 from the symmetry-related molecule makes specific crystal contacts with the main chain amides of Val637 and His638.

Ponatinib (Figure 1B) can be unambiguously modeled in the electron density map (Figure 1C) and occupies the cleft between the N- and C-terminal lobes where ATP would otherwise bind. The interactions between ponatinib and FGFR4 are similar to those seen in the complex between ponatinib and the Bcr-Abl Thr315Ile mutant (PDB accession number 3IK3) (O'Hare et al., 2009; Zhou et al., 2011). The imidazopyridazine template (see Figure 1B for nomenclature) forms a hydrogen bond to the backbone nitrogen atom of Ala553 located in the hinge, while the methylphenyl A ring occupies the hydrophobic pocket located behind the gatekeeper residue, Val550. Critical to the binding of ponatinib is a conformational rearrangement of the conserved Asp630-Phe631-Gly632 (DFG) tripeptide motif at the proximal end of the activation loop. In the complex of ponatinib with FGFR4, the side chain of Phe631 is flipped out toward the solvent, thereby creating an induced-fit hydrophobic pocket into which the trifluoromethylphenyl B ring binds. This observation of the DFG-out activation loop conformation in the FGFR kinase family confirms ponatinib as a type II FGFR inhibitor. The amide connecting the A and B rings (linker 2) is involved in a pair of hydrogen bond interactions with the backbone nitrogen atom of Asp630 from the DFG motif and the side chain of the strictly conserved glutamate of the αC-helix (Glu520), which is characteristic of a type II inhibitor (Liu and Gray, 2006). The distance between the terminal piperazinyl nitrogen atom of ponatinib and the carbonyl oxygen atom of residue Ile609 in the catalytic loop is 3.0Å, suggesting that the piperazinyl nitrogen atom is protonated such that the tertiary ammonium ion forms a hydrogen bond.

The Structure of FGFR1 in Complex with Ponatinib Confirms the Propensity of FGFRs to Adopt a DFG-Out Binding Mode

In order to ascertain whether the DFG-out activation loop conformation is more generally accessible to FGFR kinases, we generated structures of the FGFR1 kinase domain in complex with ponatinib. We chose to work with FGFR1 because this system has been extensively characterized by us, from both structural and biophysical perspectives (Klein et al., 2014; Norman et al., 2012a). Structures of a crystallizable form of the FGFR1 kinase domain (Ala458 to Glu765 [Cys488A Cys584S]) in complex with ponatinib were generated using both cocrystallization and crystal-soaking protocols (Table 1; Supplemental Experimental Procedures). In both structures, there are two molecules of FGFR1 in the crystallographic asymmetric unit related by a noncrystallographic two-fold axis. The refined models consist of residues Leu465 to Glu765 of monomer A and Ser461 to Asn763 of monomer B. The two monomers are highly similar, exhibiting rmsd values of 0.38 Å over 269 Cα and 0.41 Å over 281 Cα for the soaked and cocrystallized structures, respectively. The two structures are also essentially identical (rmsd values of 0.29 Å over 273 Cα of monomers A and 0.31 Å over 275 Cα of monomers B). Interestingly, however, ponatinib is present at ~55% occupancy in the FGFR1 cocrystal structure such that both DFG-in and DFG-out conformations of the activation loop can be visualized simultaneously. In contrast, the DFG-out conformation is observed at 100% occupancy in the FGFR1 structure, which was obtained by soaking of ponatinib, suggesting that this crystal form is compatible with the protein movements required to achieve the DFG-in/DFG-out flip. Further discussion will therefore refer to monomer A from the higher occupancy structure obtained by soaking ponatinib, except where specifically indicated otherwise.

In contrast to the structure of FGFR4 in complex with ponatinib, the activation loop and the P loop of the FGFR1-ponatinib complex structure are only partially resolved in the electron density map. P loop residues Glu486 to Phe489 of monomer A and Ala488 to Phe489 of monomer B and activation loop residues

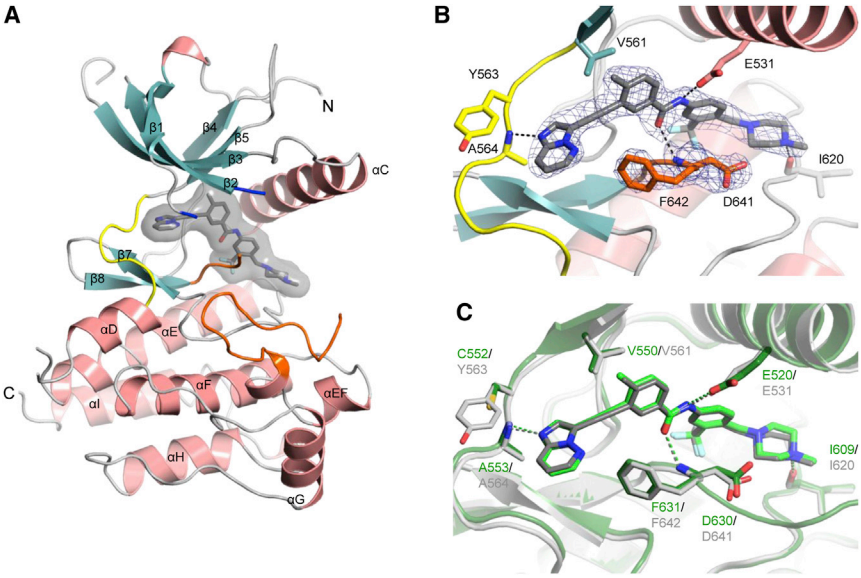

Figure 2. Crystal Structure of the Catalytic Domain of FGFR1 Kinase in Complex with Ponatinib

(A) Ribbon representation of the X-ray crystal structure of FGFR1 in complex with ponatinib (carbon atoms in gray, van der Waals surface representation also shown) obtained by soaking, labeled and colored as in Figure 1A.

(B) Active site of FGFR1 kinase in complex with ponatinib (carbon atoms in gray) as determined at 2.33 Å resolution. $F_o - F_c$ OMIT electron density and polar interactions are represented as in Figure 1C.

(C) Overlay of the active sites of FGFR1 kinase (gray ribbon representation) and FGFR4 kinase (dark green ribbon representation) in complex with ponatinib (carbon atoms in gray and green respectively).

In (B) and (C), selected residues are shown as sticks and labeled.

Gly643 to His650 from monomers A and B could not be modeled (Figure 2A). The features that result in the FGFR4 activation loop being ordered are not conserved in the FGFR1 crystal system. Ponatinib can be unambiguously modeled in the electron density map (Figure 2B) and, as observed for the FGFR4-ponatinib complex, binds in a type II binding mode to FGFR1 making identical interactions to those observed for FGFR4 (Figure 2C).

The Structure of FGFR1 in Complex with AZD4547 Exemplifies a Type I Inhibitor Binding Mode and Is Accompanied by P Loop Closure

AZD4547 is a potent and selective inhibitor of FGFR1, FGFR2, and FGFR3 currently in clinical trials for a variety of FGFR-driven tumors (ClinicalTrials.gov identifier NCT01457846). AZD4547 is approximately 1,000-fold more potent against FGFR1 than FGFR4 in an enzyme assay and 10-fold less potent against FGFR4 than ponatinib (see Table 2). In an attempt to rationalize these dramatic differences in FGFR isoform selectivity between ponatinib and AZD4547, we generated the structure of FGFR1 in complex with AZD4547 (Figure 3A) by soaking the compound into preformed crystals of the FGFR1 kinase domain. As observed for the FGFR1-ponatinib complex structure, there are two molecules of FGFR1 in the crystallographic asymmetric unit. The refined model consists of residues Glu464 to Glu765 of monomer A and Gly459 to Gln764 of monomer B (see Table 1 for details of crystallographic data collection and refinement statistics). The two monomers are highly similar, exhibiting rmsd values of 0.82 Å over 281 Cα and 0.26 Å over 25 Cα within 4.5 Å of the AZD4547 binding site. Further discussion will therefore refer to the structure of monomer A, except where specifically indicated otherwise.

AZD4547 (Figure 3B) occupies the ATP-binding cleft of FGFR1, as expected on the basis of previous structures of FGFR1 in complex with other pyrazole series inhibitors (Klein et al., 2014; Norman et al., 2012a) (PDB accession numbers 4F63, 4F64, 4F65, 4NK9, 4NKA, and 4NKS), and the activation loop in the FGFR1-AZD4547 complex structure exhibits a DFG-in conformation. The activation loop is only partially ordered (residues Asp647 to His650 of monomer A and Ala645 to Ile648 of monomer B could not be modeled), but the conformation of the DFG motif is clearly defined (Figure 3C). The pyrazole amide template forms three hydrogen bonds to the hinge region, while the dimethoxyphenyl A ring occupies the hydrophobic pocket located behind the gatekeeper residue (Val561). One of the methoxy oxygen atoms is involved in a hydrogen bond with the backbone nitrogen atom of the DFG aspartate (Asp641), mimicking the A ring and linker 1 amide interactions of ponatinib (Figure 3D). As observed for other compounds of the pyrazole series (PDB accession numbers 4F65, 4NK9, and 4NKS) and the potent inhibitor PD173074 (PDB accession number 2FGI), AZD4547 binds to FGFR1 with the plane of the 3,5-dimethoxyphenyl ring approximately perpendicular to the plane of the template. The dimethylpiperazinylphenyl solubilizing group extends away from the hinge region toward the solvent channel and does not make any specific interactions with the protein. The P loop is well ordered in both monomers and, as previously reported (Klein et al., 2014; Simard et al., 2010), adopts a "closed" conformation (Figure 3B) that shields the ligand from the surrounding solvent. The side chain of Phe489 from the tip of the P loop stacks against the dimethoxyphenyl A-ring in a parallel displaced conformation and occupies a constricted indentation at the base of the ATP-binding pocket (residues Asn628, Leu630, and Ala640), which was previously referred to as the "pit" region (Norman et al., 2012a). Interestingly, in complexes with those compounds of the pyrazole series which contain a methyl isoxazole moiety, this latter moiety is also observed to occupy the FGFR1 pit region (PDB accession numbers 4F64, 4F65, 4NK9, 4NKA, and 4NKS).

Structural and Biophysical Comparison of FGFR1 and FGFR4 with Bound Ponatinib and AZD4547 Sheds Light on Isoform Selectivity Differences

There are two differences in sequence between FGFR isoforms 1 to 3 and FGFR4 in the vicinity of the AZD4547 and ponatinib binding sites. Residue Leu494, located at the C-terminal end of the P loop in FGFR1, is a methionine in FGFR2 (Met497) and

Table 2. Binding Kinetic and Biochemical Inhibition Data for Ponatinib and AZD4547 toward FGFR1 and FGFR4 Kinase Domains

	AZD4547	Ponatinib
FGFR1		
k_{on} (M^{-1} s^{-1})	$2.5 \times 10^7 \pm 3.2 \times 10^5$[a]	$2.4 \times 10^4 \pm 1.4 \times 10^1$
k_{off} (s^{-1})	$6.0 \times 10^{-3} \pm 1.2 \times 10^{-4}$	$1.8 \times 10^{-4} \pm 7.7 \times 10^{-8}$
K_D (nM)	0.2 ± 0.01	7.7 ± 0.03
pIC_{50}	9.7	8.9 (8.7)
FGFR4		
k_{on} (M^{-1} s^{-1})	$\geq 1.0 \times 10^8$[b]	$2.8 \times 10^4 \pm 2.9 \times 10^1$
k_{off} (s^{-1})	$\geq 8.5 \times 10^{-1}$[b]	$4.4 \times 10^{-4} \pm 1.1 \times 10^{-6}$
K_D (nM)	17.1 ± 0.9[c]	16.0 ± 0.04
pIC_{50}	6.8	7.7 (8.1)

See also Figures S2 and S3. SPR experiments were performed at 298 K. Equilibrium dissociation constants (k_{on}/k_{off}). Potency data presented as pIC_{50} ($pIC_{50} = -\log10[IC_{50}]$); values in parentheses represent the potency data for ponatinib published by ARIAD Pharmaceuticals (Gozgit et al., 2012); data for AZD4547 were retrieved from Gavine et al. (2012).
[a] k_{on} is approaching the limit that can be measured by the instrument.
[b] Kinetic rate constants are outside the limits that can be measured by the instrument.
[c] K_D was determined from dosage experiments, and binding responses at equilibrium were fit to a 1:1 steady-state affinity. Data represent geometric mean ± SE from at least two independent experiments.

FGFR3 (Met488) and an arginine in FGFR4 (Arg483). The tyrosine central to the hinge in FGFR1 (Tyr563), FGFR2 (Tyr566), and FGFR3 (Tyr557) is replaced by Cys552 in FGFR4 (Figure 3D). Neither of these residues is involved in direct interactions with either inhibitor, although the side chain of Tyr563 may contribute to hydrophobic packing against the imidazopyridazine and the pyrazole amide templates of ponatinib and AZD4547, respectively. By analogy with the inferences drawn from the effects of mutations in the hinge region on the potency and sensitivity of ponatinib for Bcr-Abl mutants (Zhou et al., 2011), loss of an aromatic side chain in the hinge might be expected to reduce affinity for ponatinib. Consistent with this hypothesis, we observed a 2-fold reduction in binding affinity (K_D) for ponatinib when comparing FGFR1 and FGFR4 (Table 2).

Given the similarities in the binding sites of FGFR4 and FGFR1, we were unable to fully explain the differences in behavior of ponatinib and AZD4547 toward each isoform using our structural data alone. Thus, we sought to complement these data with solution-based kinetic characterization of ponatinib and AZD4547 to the isolated kinase domains of FGFR1 and FGFR4 using SPR (Table 2). Our kinetic analysis highlights the binding of ponatinib to FGFR1 as exceptionally slow. With an association rate constant of 2.4×10^4 M^{-1} s^{-1}, it is as much as 3 orders of magnitude slower than that of AZD4547 ($k_{on} = 2.5 \times 10^7$ M^{-1} s^{-1}). Notably, the high binding affinity of ponatinib to FGFR1 is a result of the extraordinary stability of the FGFR1-ponatinib complex: the dissociation rate constant for ponatinib ($k_{off} = 1.8 \times 10^{-4}$ s^{-1}) is approximately 33-fold slower than that for AZD4547 ($k_{off} = 6.0 \times 10^{-3}$ s^{-1}). The binding of ponatinib to FGFR4 is also characterized by slow kinetic rate constants, which are fairly similar to those observed for the binding of ponatinib to FGFR1. Hence, ponatinib shows comparable binding affinities toward FGFR1 (K_D = 7.7 nM) and FGFR4 (K_D = 16 nM), and these are in agreement with the reported inhibitory potencies (Table 2; Gozgit et al., 2012). In contrast, the binding affinities of AZD4547 for FGFR1 and FGFR4 differ by almost 2 orders of magnitude (FGFR1 K_D = 0.2 nM, FGFR4 K_D = 17.1 nM). The kinetic constants for AZD4547 binding to FGFR4 are outside the limits that can be measured by the instrument used in this study, but they clearly indicate that a low FGFR4-AZD4547 complex stability (fast on and off rates) is the key driver for the reduced affinity of AZD4547 toward FGFR4 compared with FGFR1. The observed differences in the AZD4547 binding affinities are again consistent with the inhibitory potencies derived from the biochemical assay (Table 2; Gavine et al., 2012). The slow kinetic rate constants observed with ponatinib are in line with those observed for p38 with the type II inhibitor BIRB-796 ($k_{on} = 5 \times 10^4$ M^{-1} s^{-1}, $k_{off} = 5.0 \times 10^{-5}$ s^{-1}, K_D = 1.0 nM) (Schreiber et al., 2006). These rate constants were further optimized in the design of the p38 inhibitor PF-03715455 ($k_{on} = 3 \times 10^6$ M^{-1} s^{-1}, $k_{off} = 2.4 \times 10^{-6}$ s^{-1}, K_D = 0.001 nM) (Millan et al., 2011), suggesting that type II inhibitors of FGFRs more potent than ponatinib can be designed.

Mapping of Somatic Mutations on the Structure of FGFR4 Rationalizes Their Effects on Kinase Activity and Sensitivity to Ponatinib Inhibition

Four sites of somatic mutation in the FGFR4 kinase domain have been identified in human RMS samples (Taylor et al., 2009). Two of these, Asn535Lys and Val550Glu, were further demonstrated to have an activating effect on FGFR4 activity in cell-based assays. The remaining mutations (Asn535Asp, Val550Leu, Ala554Val, and Gly576Asp) were not experimentally characterized, but computational methods suggested that they would affect FGFR4 kinase function. A number of additional somatic mutations have been identified in breast and lung cancer samples, including Val550Met, the functional effects of which have not been described (Davies et al., 2005; Ding et al., 2008; Greenman et al., 2007). We sought to understand the effects these mutations might have on the kinase activity of FGFR4, and sensitivity to ponatinib inhibition, by mapping them onto our FGFR4-ponatinib crystal structure (Figure 4A).

Three mutation sites (535, 550, and 554) cluster in the vicinity of the ATP-binding cleft. Asn535 is completely conserved across FGFR isoforms and is located in a loop region implicated as part of the "molecular brake" that regulates FGFR basal activity (Chen et al., 2007). As reported recently for FGFR2 and FGFR3 (Chen et al., 2013), mutation of this side chain to Lys or Asp would be predicted to disrupt a network of hydrogen bonds that otherwise restrict interlobe flexibility, thus increasing the population of kinase in the active state. Interestingly, in our FGFR4-ponatinib structure, the network of hydrogen bonds that would otherwise constitute the molecular brake is partially disengaged in the absence of any mutation. The side chain of Asn535 is rotated with respect to the conformation observed for the equivalent residue (Asn546) in monomer A of the FGFR1-ponatinib structure so as to form hydrogen bonds with the side-chain of Glu551 (Glu562 in FGFR1) and a water molecule rather than to the backbone of His530 and Ile533 (His541 and Ile544, respectively, in FGFR1) (Figure 4B). In monomer B of the FGFR1-ponatinib structure, the side chain of Asn535 has been modeled in two conformations. In one of these, the network

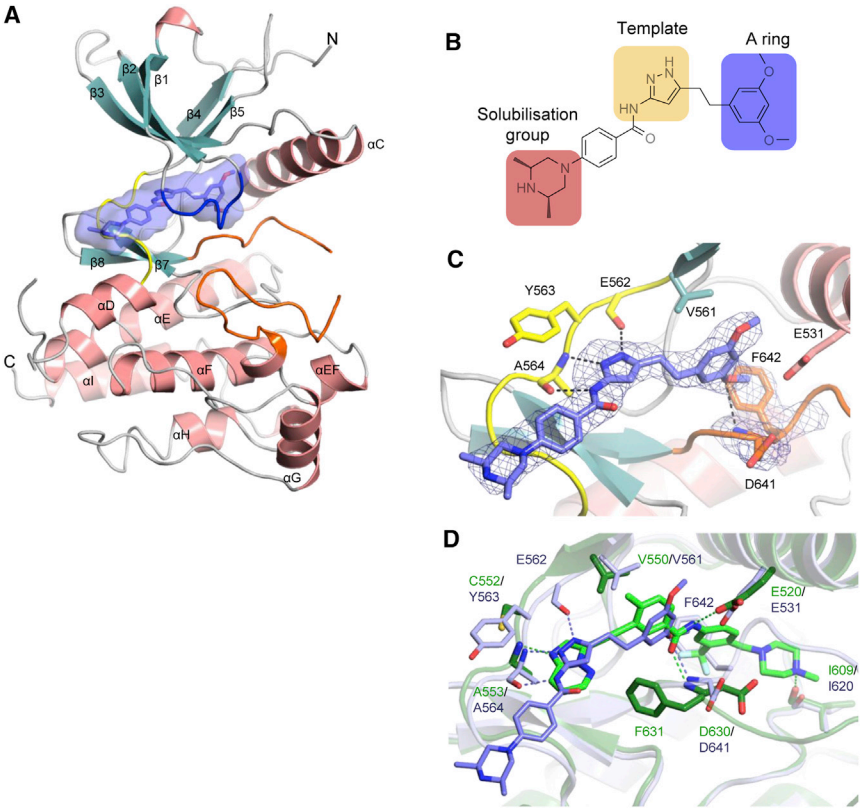

Figure 3. Crystal Structure of the Catalytic Domain of FGFR1 Kinase in Complex with AZD4547

(A) Ribbon representation of the X-ray crystal structure of FGFR1 in complex with AZD4547 (carbon atoms in slate), labeled and colored as in Figure 1A.

(B) 2D chemical representation of AZD4547, which is composed of several motifs designated as the (pyrazole amide) template, the (dimethoxyphenyl) A ring, and the (dimethylpiperazinylphenyl) solubilizing group.

(C) Active site of FGFR1 kinase in complex with AZD4547 (carbon atoms in slate) as determined at 2.57 Å resolution. $F_o - F_c$ OMIT electron density for AZD4547, the DFG motif and polar interactions are represented as in Figure 1C.

(D) Overlay of the active sites of FGFR1 kinase (light blue ribbon representation) in complex with AZD4547 (carbon atoms in slate) and FGFR4 kinase (dark green ribbon representation) in complex with ponatinib (carbon atoms in green).

In (C) and (D), selected residues are shown as sticks and labeled. See also Figure S1.

of hydrogen bonds constituting the brake is intact (as in monomer A), while in the second, an alternative network corresponding to a disengaged brake as observed in the FGFR4-ponatinib structure is evident.

The gatekeeper residue (Val550) is also conserved across all FGFR isoforms and lies at the N terminus of the hinge region. Gatekeeper mutations in other tyrosine kinases have been shown to stabilize the hydrophobic spine (Azam et al., 2008), thus leading to enhanced kinase activity through stabilization of the active state. A similar effect is likely for the FGFR4 gatekeeper mutations where, for example, both Val550Leu and Val550Met increase the size of the gatekeeper residue, allowing improved packing. As expected, binding of ponatinib to FGFR4 and FGFR1 disrupts the hydrophobic spine through displacement of the Phe side chain to the DFG-out conformation (Figure 4C, left). In contrast, the FGFR1-AZD4547 structure shows an intact hydrophobic spine (Figure 4C, right). Mutation of Val550 to amino acids with bulkier side chains such as Met or Leu would be predicted to alter the sensitivity of FGFR4 to inhibitors, such as ponatinib and AZD4547, that access the pocket beyond this residue by a mechanism of steric hindrance (Figure 4D). This has been observed for the FGFR2 gatekeeper mutation Val565Ile, which confers resistance to ponatinib (Byron et al., 2013).

DISCUSSION

The X-ray crystal structures of the kinase domains of FGFR1 and FGFR4 bound to the pan-FGFR TKI ponatinib presented here show that both FGFR isoforms bind the inhibitor in a type II, DFG-out binding mode, similar to that observed for its originally reported target Bcr-Abl. This prompts the question of whether the apparently refractory nature of FGFRs toward adoption of the DFG-out conformation lies at the level of the protein itself or is more a function of an exacting requirement for specific chemical interaction motifs in the inhibitor. The ponatinib-binding mode contrasts with that of the archetypal type I pose adopted by AZD4547, whose structure we have determined in complex with FGFR1 and present here. Our data comparing the distinct binding modes of these two inhibitors reveal that the potencies exhibited for the two FGFR isoforms cannot be fully explained by structural comparison alone. Our kinetic characterization of ponatinib and AZD4547 binding to FGFR1 and FGFR4 reveals dramatic differences in the association and dissociation rates between the two TKIs; ponatinib binds and dissociates up to 100-fold more slowly than AZD4547. These slow binding kinetics suggest the existence of a high-energy barrier to the attainment of the DFG-out protein conformation and/or may indicate a requirement for ponatinib to rearrange to a less energetically favorable conformation in order to allow binding to the predominant kinase conformation in solution. Further detailed mechanistic investigations, together with insights into the underlying protein conformational dynamics derived from nuclear magnetic resonance relaxation studies, will be required to develop a complete picture of the factors governing the DFG-flip in FGFRs. Work to further elucidate the role of dynamics is ongoing in our laboratory and will be described elsewhere.

Mechanistic characterization of disease-associated mutations in FGFRs has highlighted the importance of the molecular brake and the role of a key conserved asparagine residue (Asn535 in FGFR4) in maintaining the kinase in the inactive state. A recent report from Byron and coworkers suggests that mutation of this residue may also alter FGFR2 sensitivity to inhibition by

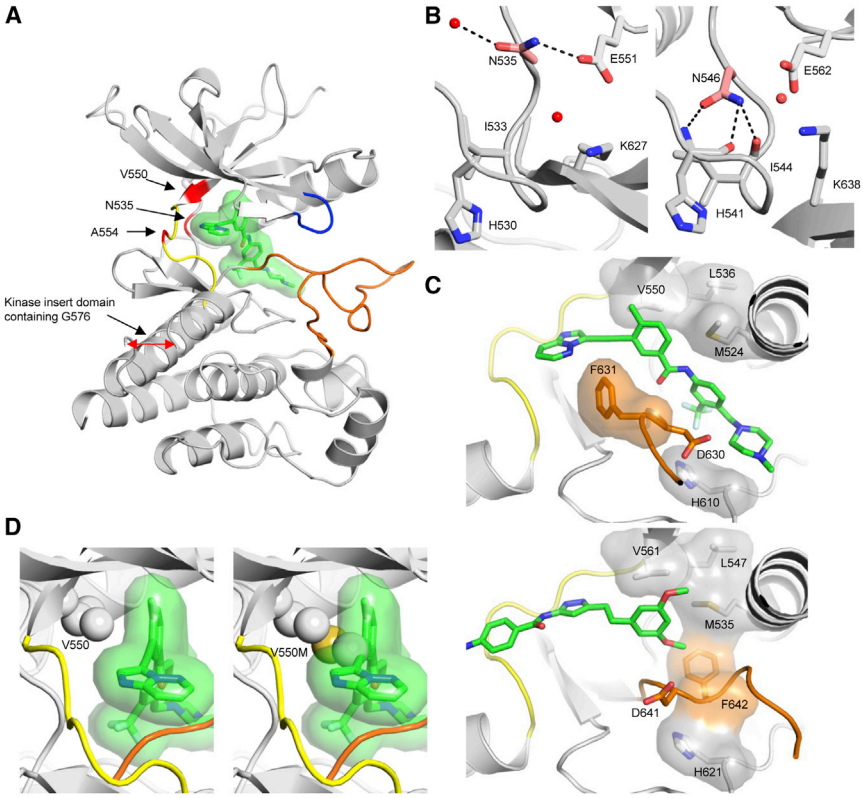

Figure 4. Structural Modeling of Somatic FGFR4 Mutations

(A) Codons 535, 550, 554, and 576 (red) mapped onto the structure of FGFR4 kinase in complex with ponatinib (colored as in Figure 1).

(B) Close-up view of the intramolecular interactions of Asn535 and neighboring residues in the FGFR4-ponatinib (left) and FGFR1-ponatinib (right) complexes.

(C) Close-up view of the disassembled hydrophobic spine (carbon atoms in gray and van der Waals surface shown) in the FGFR4-ponatinib complex (top), with the DFG phenylalanine (carbon atoms in orange and van der Waals surface shown) flipped outward to form an extended cavity for ponatinib binding. Close-up view of the intact hydrophobic spine in the FGFR1-AZD4547 complex (bottom), with the DFG phenylalanine as a key component of interlobe connectivity.

(D) Close-up view of FGFR4 gatekeeper residue (Val550, shown as atomic spheres) interaction with ponatinib (carbon atoms in green and van der Waals surface shown) (left). Close-up view of predicted steric clash between bulky gatekeeper mutant (Met550, shown as atomic spheres) with ponatinib (right).

See also Figure S1.

different classes of TKIs (Byron et al., 2013). The Asn550Lys mutation in FGFR2 conferred resistance to the type I inhibitors PD173074 and dovitinib but not to the type II TKI ponatinib. Our structures appear consistent with these data in that we observe an engaged brake in the structure of the FGFR1-AZD4547 complex, a predominantly engaged brake in the structure of the FGFR1-ponatinib complex, and a disengaged brake in the structure of FGFR4 in complex with ponatinib. Although by no means conclusive, the observed differences in the degree of molecular brake engagement among our FGFR1 and FGFR4 structures suggest the potential for greater flexibility in FGFR4, such that in solution, the FGFR4 kinase domain may sample a wider range of conformations, occupying an active-like conformation more often than FGFR1. Such a difference in dynamic behavior is consistent with our kinetic data, which show a decrease in stability for the complex of AZD4547 with FGFR4 compared with FGFR1. It would also be consistent with the reduced propensity of FGFR4 to crystallize compared with FGFR1, and the lower Tm for the FGFR4 kinase domain in the apo state (Table S1). Finally, increased conformational flexibility in FGFR4 may contribute to the potency drop-off observed for AZD4547 and other type I FGFR inhibitors, which may bind preferentially to a conformation in which the molecular brake is engaged. Further work will be required to fully elucidate these differences in conformational dynamics and understand their impact on inhibitor binding and isoform selectivity.

The demonstration that FGFR1 and FGFR4 can adopt the inactive DFG-out conformation opens new avenues for the design of novel FGFR type II kinase inhibitors with differing selectivity and kinetic profiles. Hybrid design approaches in which type I inhibitor templates are linked to type II inhibitor A ring moieties known to bind in the DFG-out pocket have proved successful in several kinase systems, notably in the development of second- and third-generation Bcr-Abl inhibitors (Liu and Gray, 2006) and p38 kinase inhibitors (Millan et al., 2011). This approach is now available for the design of next generation FGFR kinase inhibitors with longer residence times, which may provide a higher barrier to the development of chemoresistance.

Availability of the FGFR4 crystal structure has enabled us to make a detailed comparison of the active sites of FGFR1 and FGFR4. This has highlighted a key difference in the hinge region; Tyr563 in FGFR1 (also conserved in FGFR2 and FGFR3) is Cys552 in FGFR4. A recent paper by Zhou and coworkers presents the development of pan-FGFR inhibitors that covalently target the conserved Cys in the P loop (Zhou et al., 2010). Application of a similar approach to develop covalent inhibitors targeting Cys552 could be envisaged as a strategy for the design of FGFR4-selective inhibitors. Combined targeting of Cys552 and the DFG-out hydrophobic pocket could provide a means to the creation of inhibitors which are both potent and selective against FGFR4.

EXPERIMENTAL PROCEDURES

Additional details are provided in Supplemental Experimental Procedures.

Compound Synthesis

Ponatinib was purchased from Selleckchem. AZD4547 was synthesized as previously described (Gavine et al., 2012).

Kinase Inhibition Assay

The inhibitory activity of ponatinib against FGFR1 and FGFR4 kinases was determined with a Caliper off-chip incubation mobility shift assay as previously described (Norman et al., 2012a).

Thermal Shift Analysis

Thermal melting experiments using the Thermofluor technique were used to identify compounds that stabilized the FGFR4 kinase domain (Holdgate, 2007). Full details are provided in Supplemental Experimental Procedures.

Protein Expression and Purification

Human FGFR4 consisting of residues Ala447-Glu753 with an engineered N-terminal TEV protease-cleavable 6His tag and a Cys477Ala mutation was expressed in *E. coli* BL21 (DE3) GOLD. Coexpression with untagged PTP1B provided nonphosphorylated FGFR4. FGFR4 was purified by immobilized metal affinity chromatography (IMAC), TEV protease cleavage to remove the 6His tag, subtractive IMAC, and size exclusion chromatography (SEC). Human FGFR1 consisting of residues Ala458-Glu765 with an engineered TEV protease-cleavable N-terminal 6His tag and mutations Cys488Ala and Cys584Ser (Mohammadi et al., 1996) was expressed and purified as previously described (Norman et al., 2012a) with minor modifications. The 6His tag was retained on proteins destined for SPR experiments, and for FGFR4, an additional ion exchange step was used prior to the final SEC. Full details are provided in Supplemental Experimental Procedures.

Crystallization

FGFR4-Ponatinib Complex

GS-FGFR4(Ala447-Glu753)[Cys477Ala] in SEC buffer at 12 mg/mL was mixed with a 100 mM ponatinib stock solution in DMSO to give a final concentration of 1 mM ponatinib, 1% DMSO. Complex formation was allowed to proceed for 3 hours at 277 K. The sample was clarified by centrifugation (16,000 × g, 277 K, 5 min), and crystals were grown at 277 K by sitting drop vapor diffusion using a 1:1 ratio of FGFR4-ponatinib complex to precipitant, consisting of 0.1 M PCTP (pH 4.5) (0.04 M sodium propionate, 0.02 M sodium cacodylate, 0.04 M bis-tris propane), 0.1 M $(NH_4)_2SO_4$, and 15% PEG3350, to give a 400 nL drop. Crystals grew as stacked plates, appearing within 3 weeks. Crystals were passed quickly through precipitant supplemented with 20% glycerol and then flash cooled in a gaseous nitrogen stream at 100 K prior to data collection.

FGFR1 complexes were crystallized essentially as described (Norman et al., 2012a) with minor modifications, detailed in Supplemental Experimental Procedures.

X-Ray Diffraction Data Collection and Processing

FGFR4-Ponatinib Complex

X-ray diffraction data were collected from three different crystals at the European Synchrotron Radiation Facility (ESRF) and Diamond synchrotrons (Table 1). The highest resolution data from crystal 3 were compromised by poor spot shapes and ice rings and were therefore combined with the lower resolution data from crystals 1 and 2 in order to improve the data completeness and reduce the discontinuities in the electron density maps arising from systematic incompleteness in the crystal 3 data. Data were processed using XDS (Kabsch, 2010) as implemented within XIA2 (Winter et al., 2013) (Diamond data) or EDNA (Incardona et al., 2009) (ESRF data), scaled and merged using SCALA (Evans, 2006), and further processed using programs from the CCP4 suite (Winn et al., 2011).

FGFR1 Complexes

X-ray diffraction data were collected on a rotating anode generator (Rigaku FRE) equipped with a Saturn944 CCD detector. Data were integrated and scaled with d*trek (Pflugrath, 1999) or XDS and Aimless as implemented within autoPROC (Vonrhein et al., 2011). Data were further processed using programs from the CCP4 suite (Winn et al., 2011).

Structure Solution, Refinement, and Validation

Structures were solved by molecular replacement using internal FGFR1 structures as search models. Full details are provided in Supplemental Experimental Procedures. Manual model completion in Coot (Emsley et al., 2010) was interspersed with rounds of maximum-likelihood refinement in Buster (Bricogne et al., 2011) and REFMAC5 (Murshudov et al., 2011), applying TLS parameters, and noncrystallographic symmetry restraints where appropriate. Stereochemical restraints for ponatinib and AZD4547 were generated using Corina (Sadowski et al., 1994). Quality checks on the protein structures were carried out using the validation tools in Coot (Emsley et al., 2010) and MolProbity (Chen et al., 2010b), while compound stereochemistries were checked against the Cambridge Structural Database (Allen, 2002) using Mogul (Bruno et al., 2004). Final structures have been deposited in the PDB, with accession numbers given in Table 1.

All structural figures were prepared using PyMOL (Schrödinger). Rmsd values between structures were calculated using the SSM algorithm (Krissinel and Henrick, 2004) as implemented within CCP4MG (McNicholas et al., 2011).

SPR

SPR experiments were performed using the Biacore 3000 and Biacore T200 biosensors (GE Healthcare). Nitriloacetic acid (NTA) sensor chips and series S NTA sensor chips (GE Healthcare) were used. All experiments were done using PBS (pH 7.4), 50 μM EDTA, 0.05% (v/v) surfactant P20, and 1% (v/v) DMSO as running buffer. Compounds as DMSO stocks were diluted in DMSO to concentrations 100-fold higher than the final assay concentration. Finally, they were diluted 1:100 (v/v) in running buffer without DMSO, to achieve the target concentration resulting in a final DMSO concentration of 1% (v/v). Further experimental details are provided in Supplemental Experimental Procedures.

ACCESSION NUMBERS

The coordinates and structure factors for all structures described here have been deposited in the PDB under accession numbers 4V01, 4V04, 4V05, and 4UXQ. Details are listed in Table 1.

SUPPLEMENTAL INFORMATION

Supplemental Information includes Supplemental Experimental Procedures, three figures, and one table and can be found with this article online at http://dx.doi.org/10.1016/j.str.2014.09.019.

AUTHOR CONTRIBUTIONS

J.A.T., T.K., A.L.B., R.O., and R.A.N. designed the research. J.A.T., T.K., J.B., R.O., C.P., and R.A.N. performed the research. J.A.T., T.K., J.B., R.O., C.P., and R.A.N. analyzed the data. J.A.T., T.K., J.B., A.L.B., C.P., and R.A.N. wrote the paper. All authors have given approval to the final version of the manuscript.

ACKNOWLEDGMENTS

We would like to acknowledge Claire Brassington for advice on crystallization, Jan Griesbach for expression and purification of FGFR1, Hannah Pollard for expression and purification of the FGFR4 protein used for SPR experiments, Alessandro Caputo for assistance with expression and purification of the phosphorylated FGFR4 proteins used in preliminary structural studies, and both the ESRF, Grenoble, and Diamond Light Source, Oxfordshire, for access to beam time.

Received: July 19, 2014
Revised: September 19, 2014
Accepted: September 24, 2014
Published: November 20, 2014

REFERENCES

Allen, F.H. (2002). The Cambridge Structural Database: a quarter of a million crystal structures and rising. Acta Crystallogr. B *58*, 380–388.

Azam, M., Seeliger, M.A., Gray, N.S., Kuriyan, J., and Daley, G.Q. (2008). Activation of tyrosine kinases by mutation of the gatekeeper threonine. Nat. Struct. Mol. Biol. *15*, 1109–1118.

Bange, J., Prechtl, D., Cheburkin, Y., Specht, K., Harbeck, N., Schmitt, M., Knyazeva, T., Müller, S., Gärtner, S., Sures, I., et al. (2002). Cancer progression and tumor cell motility are associated with the FGFR4 Arg(388) allele. Cancer Res. *62*, 840–847.

Birrer, M.J., Johnson, M.E., Hao, K., Wong, K.-K., Park, D.-C., Bell, A., Welch, W.R., Berkowitz, R.S., and Mok, S.C. (2007). Whole genome oligonucleotide-based array comparative genomic hybridization analysis identified fibroblast growth factor 1 as a prognostic marker for advanced-stage serous ovarian adenocarcinomas. J. Clin. Oncol. *25*, 2281–2287.

Bricogne, G., Blanc, E., Brandl, M., Flensburg, C., Keller, P., Paciorek, W., Roversi, P., Sharff, A., Smart, O.S., Vonrhein, C., and Womack, T.O. (2011). BUSTER version 2.11.5. (Cambridge, UK: Global Phasing).

Brooks, A.N., Kilgour, E., and Smith, P.D. (2012). Molecular pathways: fibroblast growth factor signaling: a new therapeutic opportunity in cancer. Clin. Cancer Res. *18*, 1855–1862.

Bruno, I.J., Cole, J.C., Kessler, M., Luo, J., Motherwell, W.D.S., Purkis, L.H., Smith, B.R., Taylor, R., Cooper, R.I., Harris, S.E., and Orpen, A.G. (2004). Retrieval of crystallographically-derived molecular geometry information. J. Chem. Inf. Comput. Sci. *44*, 2133–2144.

Byron, S.A., Chen, H., Wortmann, A., Loch, D., Gartside, M.G., Dehkhoda, F., Blais, S.P., Neubert, T.A., Mohammadi, M., and Pollock, P.M. (2013). The N550K/H mutations in FGFR2 confer differential resistance to PD173074, dovitinib, and ponatinib ATP-competitive inhibitors. Neoplasia *15*, 975–988.

Chen, H., Ma, J., Li, W., Eliseenkova, A.V., Xu, C., Neubert, T.A., Miller, W.T., and Mohammadi, M. (2007). A molecular brake in the kinase hinge region regulates the activity of receptor tyrosine kinases. Mol. Cell *27*, 717–730.

Chen, G., Tian, X., Liu, Z., Zhou, S., Schmidt, B., Henne-Bruns, D., Bachem, M., and Kornmann, M. (2010a). Inhibition of endogenous SPARC enhances pancreatic cancer cell growth: modulation by FGFR1-III isoform expression. Br. J. Cancer *102*, 188–195.

Chen, V.B., Arendall, W.B., 3rd, Headd, J.J., Keedy, D.A., Immormino, R.M., Kapral, G.J., Murray, L.W., Richardson, J.S., and Richardson, D.C. (2010b). MolProbity: all-atom structure validation for macromolecular crystallography. Acta Crystallogr. D Biol. Crystallogr. *66*, 12–21.

Chen, H., Huang, Z., Dutta, K., Blais, S., Neubert, T.A., Li, X., Cowburn, D., Traaseth, N.J., and Mohammadi, M. (2013). Cracking the molecular origin of intrinsic tyrosine kinase activity through analysis of pathogenic gain-of-function mutations. Cell Rep. *4*, 376–384.

Davies, H., Hunter, C., Smith, R., Stephens, P., Greenman, C., Bignell, G., Teague, J., Butler, A., Edkins, S., Stevens, C., et al. (2005). Somatic mutations of the protein kinase gene family in human lung cancer. Cancer Res. *65*, 7591–7595.

Desnoyers, L.R., Pai, R., Ferrando, R.E., Hötzel, K., Le, T., Ross, J., Carano, R., D'Souza, A., Qing, J., Mohtashemi, I., et al. (2008). Targeting FGF19 inhibits tumor growth in colon cancer xenograft and FGF19 transgenic hepatocellular carcinoma models. Oncogene *27*, 85–97.

Ding, L., Getz, G., Wheeler, D.A., Mardis, E.R., McLellan, M.D., Cibulskis, K., Sougnez, C., Greulich, H., Muzny, D.M., Morgan, M.B., et al. (2008). Somatic mutations affect key pathways in lung adenocarcinoma. Nature *455*, 1069–1075.

Emsley, P., Lohkamp, B., Scott, W.G., and Cowtan, K. (2010). Features and development of Coot. Acta Crystallogr. D Biol. Crystallogr. *66*, 486–501.

Evans, P. (2006). Scaling and assessment of data quality. Acta Crystallogr. D Biol. Crystallogr. *62*, 72–82.

French, D.M., Lin, B.C., Wang, M., Adams, C., Shek, T., Hötzel, K., Bolon, B., Ferrando, R., Blackmore, C., Schroeder, K., et al. (2012). Targeting FGFR4 inhibits hepatocellular carcinoma in preclinical mouse models. PLoS ONE *7*, e36713.

Gavine, P.R., Mooney, L., Kilgour, E., Thomas, A.P., Al-Kadhimi, K., Beck, S., Rooney, C., Coleman, T., Baker, D., Mellor, M.J., et al. (2012). AZD4547: an orally bioavailable, potent, and selective inhibitor of the fibroblast growth factor receptor tyrosine kinase family. Cancer Res. *72*, 2045–2056.

Goetz, R., and Mohammadi, M. (2013). Exploring mechanisms of FGF signalling through the lens of structural biology. Nat. Rev. Mol. Cell Biol. *14*, 166–180.

Gozgit, J.M., Wong, M.J., Moran, L., Wardwell, S., Mohemmad, Q.K., Narasimhan, N.I., Shakespeare, W.C., Wang, F., Clackson, T., and Rivera, V.M. (2012). Ponatinib (AP24534), a multitargeted pan-FGFR inhibitor with activity in multiple FGFR-amplified or mutated cancer models. Mol. Cancer Ther. *11*, 690–699.

Greenman, C., Stephens, P., Smith, R., Dalgliesh, G.L., Hunter, C., Bignell, G., Davies, H., Teague, J., Butler, A., Stevens, C., et al. (2007). Patterns of somatic mutation in human cancer genomes. Nature *446*, 153–158.

Greulich, H., and Pollock, P.M. (2011). Targeting mutant fibroblast growth factor receptors in cancer. Trends Mol. Med. *17*, 283–292.

Hart, K.C., Robertson, S.C., Kanemitsu, M.Y., Meyer, A.N., Tynan, J.A., and Donoghue, D.J. (2000). Transformation and Stat activation by derivatives of FGFR1, FGFR3, and FGFR4. Oncogene *19*, 3309–3320.

Ho, H.K., Pok, S., Streit, S., Ruhe, J.E., Hart, S., Lim, K.S., Loo, H.L., Aung, M.O., Lim, S.G., and Ullrich, A. (2009). Fibroblast growth factor receptor 4 regulates proliferation, anti-apoptosis and alpha-fetoprotein secretion during hepatocellular carcinoma progression and represents a potential target for therapeutic intervention. J. Hepatol. *50*, 118–127.

Ho, H.K., Yeo, A.H.L., Kang, T.S., and Chua, B.T. (2014). Current strategies for inhibiting FGFR activities in clinical applications: opportunities, challenges and toxicological considerations. Drug Discov. Today *19*, 51–62.

Holdgate, G.A. (2007). Thermodynamics of binding interactions in the rational drug design process. Exp. Opin. Drug Discov. *2*, 1103–1114.

Huang, Z., Chen, H., Blais, S., Neubert, T.A., Li, X., and Mohammadi, M. (2013). Structural mimicry of a-loop tyrosine phosphorylation by a pathogenic FGF receptor 3 mutation. Structure *21*, 1889–1896.

Incardona, M.-F., Bourenkov, G.P., Levik, K., Pieritz, R.A., Popov, A.N., and Svensson, O. (2009). EDNA: a framework for plugin-based applications applied to X-ray experiment online data analysis. J. Synchrotron Radiat. *16*, 872–879.

Jang, J.-H., Shin, K.-H., and Park, J.-G. (2001). Mutations in fibroblast growth factor receptor 2 and fibroblast growth factor receptor 3 genes associated with human gastric and colorectal cancers. Cancer Res. *61*, 3541–3543.

Kabsch, W. (2010). XDS. Acta Crystallogr. D Biol. Crystallogr. *66*, 125–132.

Klein, T., Tucker, J., Holdgate, G.A., Norman, R.A., and Breeze, A.L. (2014). FGFR1 kinase inhibitors: close regioisomers adopt divergent binding modes and display distinct biophysical signatures. ACS Med. Chem. Lett. *5*, 166–171.

Kornev, A.P., Haste, N.M., Taylor, S.S., and Eyck, L.F. (2006). Surface comparison of active and inactive protein kinases identifies a conserved activation mechanism. Proc. Natl. Acad. Sci. USA *103*, 17783–17788.

Krissinel, E., and Henrick, K. (2004). Secondary-structure matching (SSM), a new tool for fast protein structure alignment in three dimensions. Acta Crystallogr. D Biol. Crystallogr. *60*, 2256–2268.

Kurosu, H., Choi, M., Ogawa, Y., Dickson, A.S., Goetz, R., Eliseenkova, A.V., Mohammadi, M., Rosenblatt, K.P., Kliewer, S.A., and Kuro-o, M. (2007). Tissue-specific expression of betaKlotho and fibroblast growth factor (FGF) receptor isoforms determines metabolic activity of FGF19 and FGF21. J. Biol. Chem. *282*, 26687–26695.

Laskowski, R.A., MacArthur, M.W., Moss, D.S., and Thornton, J.M. (1993). *PROCHECK*: a program to check the stereochemical quality of protein structures. J. Appl. Cryst. *26*, 283–291.

Lin, B.C., Wang, M., Blackmore, C., and Desnoyers, L.R. (2007). Liver-specific activities of FGF19 require Klotho beta. J. Biol. Chem. *282*, 27277–27284.

Liu, Y., and Gray, N.S. (2006). Rational design of inhibitors that bind to inactive kinase conformations. Nat. Chem. Biol. *2*, 358–364.

Liu, Y., Shah, K., Yang, F., Witucki, L., and Shokat, K.M. (1998). A molecular gate which controls unnatural ATP analogue recognition by the tyrosine kinase v-Src. Bioorg. Med. Chem. *6*, 1219–1226.

McNicholas, S., Potterton, E., Wilson, K.S., and Noble, M.E.M. (2011). Presenting your structures: the CCP4mg molecular-graphics software. Acta Crystallogr. D Biol. Crystallogr. *67*, 386–394.

Mellor, H.R. (2014). Targeted inhibition of the FGF19-FGFR4 pathway in hepatocellular carcinoma; translational safety considerations. Liver Int. *34*, e1–e9.

Millan, D.S., Bunnage, M.E., Burrows, J.L., Butcher, K.J., Dodd, P.G., Evans, T.J., Fairman, D.A., Hughes, S.J., Kilty, I.C., Lemaitre, A., et al. (2011). Design and synthesis of inhaled p38 inhibitors for the treatment of chronic obstructive pulmonary disease. J. Med. Chem. *54*, 7797–7814.

Mohammadi, M., Schlessinger, J., and Hubbard, S.R. (1996). Structure of the FGF receptor tyrosine kinase domain reveals a novel autoinhibitory mechanism. Cell *86*, 577–587.

Murshudov, G.N., Skubák, P., Lebedev, A.A., Pannu, N.S., Steiner, R.A., Nicholls, R.A., Winn, M.D., Long, F., and Vagin, A.A. (2011). REFMAC5 for the refinement of macromolecular crystal structures. Acta Crystallogr. D Biol. Crystallogr. *67*, 355–367.

Niesen, F.H., Berglund, H., and Vedadi, M. (2007). The use of differential scanning fluorimetry to detect ligand interactions that promote protein stability. Nat. Protoc. *2*, 2212–2221.

Norman, R.A., Schott, A.-K., Andrews, D.M., Breed, J., Foote, K.M., Garner, A.P., Ogg, D., Orme, J.P., Pink, J.H., Roberts, K., et al. (2012a). Protein-ligand crystal structures can guide the design of selective inhibitors of the FGFR tyrosine kinase. J. Med. Chem. *55*, 5003–5012.

Norman, R.A., Toader, D., and Ferguson, A.D. (2012b). Structural approaches to obtain kinase selectivity. Trends Pharmacol. Sci. *33*, 273–278.

O'Hare, T., Eide, C.A., and Deininger, M.W. (2007). Bcr-Abl kinase domain mutations, drug resistance, and the road to a cure for chronic myeloid leukemia. Blood *110*, 2242–2249.

O'Hare, T., Shakespeare, W.C., Zhu, X., Eide, C.A., Rivera, V.M., Wang, F., Adrian, L.T., Zhou, T., Huang, W.-S., Xu, Q., et al. (2009). AP24534, a pan-BCR-ABL inhibitor for chronic myeloid leukemia, potently inhibits the T315I mutant and overcomes mutation-based resistance. Cancer Cell *16*, 401–412.

Pai, R., French, D., Ma, N., Hotzel, K., Plise, E., Salphati, L., Setchell, K.D.R., Ware, J., Lauriault, V., Schutt, L., et al. (2012). Antibody-mediated inhibition of fibroblast growth factor 19 results in increased bile acids synthesis and ileal malabsorption of bile acids in cynomolgus monkeys. Toxicol. Sci. *126*, 446–456.

Pflugrath, J.W. (1999). The finer things in X-ray diffraction data collection. Acta Crystallogr. D Biol. Crystallogr. *55*, 1718–1725.

Roidl, A., Foo, P., Wong, W., Mann, C., Bechtold, S., Berger, H.J., Streit, S., Ruhe, J.E., Hart, S., Ullrich, A., and Ho, H.K. (2010). The FGFR4 Y367C mutant is a dominant oncogene in MDA-MB453 breast cancer cells. Oncogene *29*, 1543–1552.

Ruhe, J.E., Streit, S., Hart, S., Wong, C.-H., Specht, K., Knyazev, P., Knyazeva, T., Tay, L.S., Loo, H.L., Foo, P., et al. (2007). Genetic alterations in the tyrosine kinase transcriptome of human cancer cell lines. Cancer Res. *67*, 11368–11376.

Sadowski, J., Gasteiger, J., and Klebe, G. (1994). Comparison of automatic three-dimensional model builders using 639 X-ray structures. J. Chem. Inf. Comput. Sci. *34*, 1000–1008.

Schreiber, S., Feagan, B., D'Haens, G., Colombel, J.F., Geboes, K., Yurcov, M., Isakov, V., Golovenko, O., Bernstein, C.N., Ludwig, D., et al.; BIRB 796 Study Group (2006). Oral p38 mitogen-activated protein kinase inhibition with BIRB 796 for active Crohn's disease: a randomized, double-blind, placebo-controlled trial. Clin. Gastroenterol. Hepatol. *4*, 325–334.

Simard, J.R., Getlik, M., Grütter, C., Schneider, R., Wulfert, S., and Rauh, D. (2010). Fluorophore labeling of the glycine-rich loop as a method of identifying inhibitors that bind to active and inactive kinase conformations. J. Am. Chem. Soc. *132*, 4152–4160.

Spinola, M., Leoni, V., Pignatiello, C., Conti, B., Ravagnani, F., Pastorino, U., and Dragani, T.A. (2005a). Functional FGFR4 Gly388Arg polymorphism predicts prognosis in lung adenocarcinoma patients. J. Clin. Oncol. *23*, 7307–7311.

Spinola, M., Leoni, V.P., Tanuma, J., Pettinicchio, A., Frattini, M., Signoroni, S., Agresti, R., Giovanazzi, R., Pilotti, S., Bertario, L., et al. (2005b). FGFR4 Gly388Arg polymorphism and prognosis of breast and colorectal cancer. Oncol. Rep. *14*, 415–419.

Taylor, J.G., 6th, Cheuk, A.T., Tsang, P.S., Chung, J.-Y., Song, Y.K., Desai, K., Yu, Y., Chen, Q.-R., Shah, K., Youngblood, V., et al. (2009). Identification of FGFR4-activating mutations in human rhabdomyosarcomas that promote metastasis in xenotransplanted models. J. Clin. Invest. *119*, 3395–3407.

Thussbas, C., Nahrig, J., Streit, S., Bange, J., Kriner, M., Kates, R., Ulm, K., Kiechle, M., Hoefler, H., Ullrich, A., and Harbeck, N. (2006). FGFR4 Arg388 allele is associated with resistance to adjuvant therapy in primary breast cancer. J. Clin. Oncol. *24*, 3747–3755.

Turkington, R.C., Longley, D.B., Allen, W.L., Stevenson, L., McLaughlin, K., Dunne, P.D., Blayney, J.K., Salto-Tellez, M., Van Schaeybroeck, S., and Johnston, P.G. (2014). Fibroblast growth factor receptor 4 (FGFR4): a targetable regulator of drug resistance in colorectal cancer. Cell Death Dis. *5*, e1046.

Turner, N., and Grose, R. (2010). Fibroblast growth factor signalling: from development to cancer. Nat. Rev. Cancer *10*, 116–129.

Vonrhein, C., Flensburg, C., Keller, P., Sharff, A., Smart, O., Paciorek, W., Womack, T., and Bricogne, G. (2011). Data processing and analysis with the autoPROC toolbox. Acta Crystallogr. D Biol. Crystallogr. *67*, 293–302.

Weinstein, M., Xu, X., Ohyama, K., and Deng, C.X. (1998). FGFR-3 and FGFR-4 function cooperatively to direct alveogenesis in the murine lung. Development *125*, 3615–3623.

Winn, M.D., Ballard, C.C., Cowtan, K.D., Dodson, E.J., Emsley, P., Evans, P.R., Keegan, R.M., Krissinel, E.B., Leslie, A.G.W., McCoy, A., et al. (2011). Overview of the CCP4 suite and current developments. Acta Crystallogr. D Biol. Crystallogr. *67*, 235–242.

Winter, G., Lobley, C.M.C., and Prince, S.M. (2013). Decision making in xia2. Acta Crystallogr. D Biol. Crystallogr. *69*, 1260–1273.

Wu, X., Ge, H., Lemon, B., Vonderfecht, S., Weiszmann, J., Hecht, R., Gupte, J., Hager, T., Wang, Z., Lindberg, R., and Li, Y. (2010). FGF19-induced hepatocyte proliferation is mediated through FGFR4 activation. J. Biol. Chem. *285*, 5165–5170.

Ye, Y.W., Zhou, Y., Yuan, L., Wang, C.M., Du, C.Y., Zhou, X.Y., Zheng, B.Q., Cao, X., Sun, M.H., Fu, H., and Shi, Y.Q. (2011). Fibroblast growth factor receptor 4 regulates proliferation and antiapoptosis during gastric cancer progression. Cancer *117*, 5304–5313.

Zaid, T.M., Yeung, T.-L., Thompson, M.S., Leung, C.S., Harding, T., Co, N.N., Schmandt, R.S., Kwan, S.Y., Rodriguez-Aguay, C., Lopez-Berestein, G., et al. (2013). Identification of FGFR4 as a potential therapeutic target for advanced-stage, high-grade serous ovarian cancer. Clin. Cancer Res. *19*, 809–820.

Zhou, W., Hur, W., McDermott, U., Dutt, A., Xian, W., Ficarro, S.B., Zhang, J., Sharma, S.V., Brugge, J., Meyerson, M., et al. (2010). A structure-guided approach to creating covalent FGFR inhibitors. Chem. Biol. *17*, 285–295.

Zhou, T., Commodore, L., Huang, W.-S., Wang, Y., Thomas, M., Keats, J., Xu, Q., Rivera, V.M., Shakespeare, W.C., Clackson, T., et al. (2011). Structural mechanism of the Pan-BCR-ABL inhibitor ponatinib (AP24534): lessons for overcoming kinase inhibitor resistance. Chem. Biol. Drug Des. *77*, 1–11.

Note Added in Proof

While this paper was in proof, two further publications have emerged presenting the crystal structure of the FGFR4 kinase domain in complex with ponatinib. Both of these structures display a high similarity to the FGFR4-ponatinib structure presented here and show that the activation loop adopts a DFG-out conformation. Based on the analysis of the structures presented in these publications, the authors draw similar conclusions to ours regarding the future design of FGFR4 selective inhibitors.

Lesca, E., Lammens, A., Huber, R., and Augustin, M. (2014). Structural analysis of the human fibroblast growth factor receptor 4 kinase. J. Mol. Biol. *426*, 3744–3756.

Huang, Z., Tan, L. Wang, H., Liu, Y., Blais, S., Deng, J., Neubert, T.A., Gray, N.S., Li, X., and Mohammadi, M. (2014). DFG-out mode of inhibition by an irreversible type-1 inhibitor capable of overcoming gate-keeper mutations in FGF receptors. ACS Chem. Biol. Published online October 27, 2014. http://dx.doi.org/10.1021/cb500674s.

